A physical tool for severe accident mitigation studies

N. Marie, A. Bachrata, J.M. Seiler, F. Barjot, A. Marrel, Stéphane S. Gossé, Frédéric Bertrand

A PHYSICAL TOOL FOR SEVERE ACCIDENT MITIGATION STUDIES

N. Marie[1] (Seiler), A. Bachrata[1], J.M. Seiler[2], F. Barjot[3], A. Marrel[1], S. Gossé[4], F. Bertrand[1]

[1] CEA,DEN,DER, F-13108 Saint Paul Lez Durance, France

[2] CEA,DEN,DTN, F-38054 Grenoble, France

[3]EDF R&D,SINETICS F-93141 Clamart, France

[4]CEA,DEN,DPC, F-91191 Gif Sur Yvette, France

Keywords: Sodium Fast Reactor, Severe accident, Mitigation, Physical approach, Safety studies.

Highlights

- Physical tool for mitigation studies devoted to SFR safety
- Physical models to describe the material discharge from core
- Comparison to SIMMER III results
- Studies for ASTRID safety assessment and support to core design.

Abstract

Within the framework of the Generation IV Sodium-cooled Fast Reactors (SFR) R&D program of CEA, the core behavior in case of severe accidents is being assessed. Such transients are usually simulated with mechanistic codes (such as SIMMER-III). As a complement to this code, which gives reference accidental transient, a physico-statistical approach is currently followed; its final objective being to derive the variability of the main results of interest for the safety. This approach involves a fast-running simulation of extended accident sequences coupling low-dimensional physical models to advanced statistical analysis techniques.

In this context, this paper presents such a low-dimensional physical tool (models and simulation results) dedicated to molten core materials discharge. This 0D tool handles heat transfers from molten (possibly boiling) pools, fuel crust evolution, phase separation/mixing of fuel/steel pools, radial thermal erosion of mitigation tubes, discharge of core materials and associated axial thermal erosion of mitigation tubes. All modules are coupled with a global neutronic evolution model of the degraded core. This physical tool is used to study and to define mitigation features (function of tubes devoted to mitigation inside the core, impact of absorbers falling into the degraded core…) to avoid energetic core recriticality during a secondary phase of a potential severe accident.

In the future, this physical tool, associated to statistical treatments of the effect of uncertainties would enable sensitivity analysis studies.

This physical tool is described before presenting its comparison against SIMMER-III code results, including a space-and energy-dependent neutron transport kinetic model, on several test cases. Then some sensitivity studies on design parameters are presented providing preliminary information for this reactor fuel oxide core design.

Corresponding author: nathalie.marie@cea.fr

Nomenclature

C_p	specific heat	[J.kg^{-1}.K^{-1}]
D_h	pool hydraulic diameter	[m]
dt	time step	[s]
e	fuel crust thickness	[m]
f	friction coefficient	[-]
g	gravity acceleration	[m.s^{-2}]
H	lower layer height	[m]
h	convective heat transfer coefficient	[W.m^{-2}.K^{-1}]
k	thermal conductivity	[W.m^{-1}.K^{-1}]
L	latent heat of vaporisation	[J.kg^{-1}]
M	molten material mass	[kg]
P	pressure	[Pa]
Power	power in the pool	[W]
S	surface / section	[m^2]
T	temperature	[K]
V_{max}	velocity of the upper surface of the lower layer	[m.s^{-1}]
ρ	density	[kg.m^{-3}]
Φ	energy	[W/m²]

Glossary

C1	inner fissile zone (not degraded)
C2	outer fissile zone (not degraded)
CRGT	control rod guide tube
CAI	lower neutronic axial protection (reflector)
CFV	low sodium void effect core (cœur à faible effet de vidange)
DCS-M-TT	mitigation complementary safety device – transfer tube
FCAI	bottom fertile zone
FCAM	median fertile zone
JSFR	Japan Sodium Fast reactor
LHS	Latin Hypercube Sampling
PLN	sodium plenum zone
PNLA	lateral neutronic protection (type A)
PNLB	lateral neutronic protection (type B)
PNS	upper neutronic protection
SFR	sodium-cooled fast reactor
ULOF	unprotected loss of flow
UTOP	unprotected transient overpower
VEI	lower gas expansion zone
VES	upper gas expansion zone

Corresponding author: nathalie.marie@cea.fr

1 Introduction

Sodium-cooled Fast Reactors (SFR) belong to the future Generation IV reactor concepts, enabling to secure the nuclear fuel resources and to manage radioactive waste. The CEA with its partners is involved in a substantial effort to define a reactor design in order to improve technology in terms of safety and reliability at an industrial scale. The core design studies are carried-out by CEA with support from AREVA, as an experienced SFR Nuclear Island engineering company and components designer, and EDF, as an experienced SFR operator. A major innovation of the new SFR French concept concerns the core which features a very low sodium void effect. This design aims at preventing a rapid power excursion and core degradation in case of a loss of coolant accident, during the primary phase of a severe accident. Thus, contrary to former fast reactor core concepts, the fissile materials would not be massively ejected during the primary phase; this would delay the risk of recriticality and accentuate the need for better controlling the mass of corium in the core region during the transition and secondary phases. That is why an enhanced safety design aiming at the elimination of severe recriticalities is adopted in this new SFR concept (Chenaud et al, 2013). Thus, in order to control and to enhance the fuel discharge from the core to the core-catcher, as already studied by Maschek et Struwe (2000) for the CAPRA cores and Yamano et al. (2012) for the JSFR, complementary safety devices for mitigation are implemented inside the core. These devices in ASTRID are called Mitigation Complementary Safety Device Transfer Tubes (called DCS-M-TT). But on the contrary to JAEA's FAIDUS concept (Yamano et al., 2012) which is a small inner duct inside sub-assemblies, these transfer tubes have the geometry of a complete sub-assembly and run across the full core support structure: the diagrid and the strongback. Assessments for this new core concept involve studies on the influence of these transfer tubes on possible severe recriticality.

In this framework of safety studies devoted to molten materials behaviour and discharge, a physical tool is being developed. As a complement to reference transients which are usually simulated with mechanistic codes such as SIMMER-III (Kondo et al, 2000), physical tools, coupled to advanced statistical technics, enable to get the variability of the main results of interest for the safety (Figure 1). Indeed, the necessary complexity of mechanistic code (gathering all models capable to simulate any accidental transient: Over-Power, Loss of Flow or Sub-Assembly Faults...) makes its use for safety-informed reactor design not feasible and it might not be straight-forward to identify the design parameters the most influential on safety. Moreover, the accidental transient could widely vary according to the state of the reactor at the accident occurrence, the features of the accident or other uncertainties. Thus, simulating only a limited number of situations could hide other situations presenting more severe consequences which could be raised during the accident transients. In this context, the development of simple, but yet accurate, physical tools is desirable owing to the need for flexibility, reduction of time consumption as well as large sensitivity analysis studies for quantifying design or safety margins.

This general approach combining a mechanistic code and physico-statistical tools has already been conducted for two accidental initiator families: the Total Instantaneous sub-assembly flow Blockage (TIB) (Marie et al. 2016) and Unprotected Loss Of Flow (ULOF) (Droin et al. 2015).

Corresponding author: nathalie.marie@cea.fr

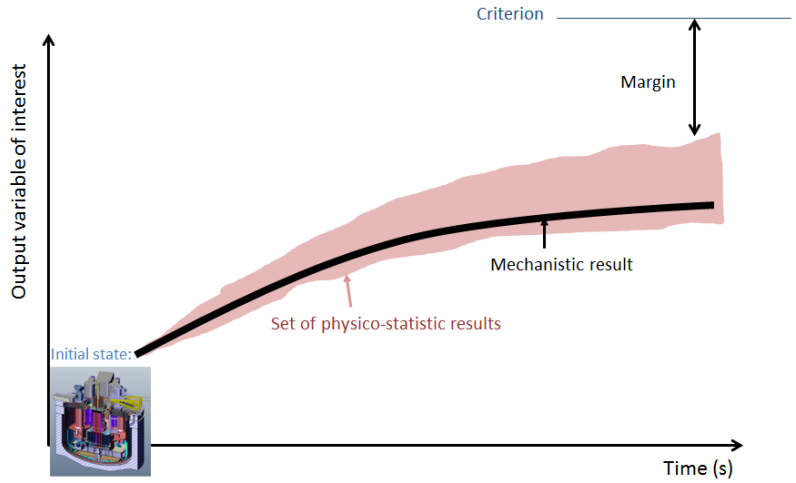

Figure 1 : Illustration of the general approach for studies – evolution of a variable of interest during the transient calculated with a mechanistic code and with a physico-statistical tool

In the present paper, the physical models of this tool dedicated to mitigation are described based on physical evidences and conservation balances. This tool handles heat transfers from molten pools to mitigation tube walls, fuel crust evolution, separation/mixing of fuel/steel pools, radial thermal erosion of tubes, and discharge of molten materials; all these models are coupled to an advanced 0D module of neutronic evolution of the fuel power. As no dedicated integral experimental results are yet available for this mitigation issue (waiting for the in-pile experiment program SAIGA (Severe Accident In-Pile experiments for Generation IV reactor and Astrid project) - Serre et al., 2015), the results of this physical tool are compared to SIMMER-III results on same transients. And finally, some sensitivity analyses to design features are given in this paper.

In the future, this tool, coupled to advanced statistical technics, will enable to assess mitigation provision need to avoid energetic core recriticality during the secondary phase of a severe accident.

2 Mitigation studies context

Core design is obviously guided by performance and safety objectives. The first safety objective is prevention of the core meltdown accident, at first through natural favourable behaviour of the core and of the reactor, and with addition of passive complementary systems if natural behaviour is not sufficient for some transient cases. The second objective is the mitigation of severe accidents to guarantee that core melting accidents do not lead to excessive mechanical energy release. The new core concept (called CFV-low sodium void effect core) is an axial heterogeneous core of 1500MWth on the contrary to more classical homogeneous cores used in former SFR. The low sodium void effect of the CFV core results mainly from the presence of a sodium plenum above the fissile zones combined to the presence of a fertile plate in the inner zone of the core encompassed by two fissile zones (displayed in Figure 2). The larger height of the outer fissile zone enables the void reactivity effect to be lowered as well, due to neutron leakage enhancement (P. Sciora et al., 2011).

Corresponding author: nathalie.marie@cea.fr

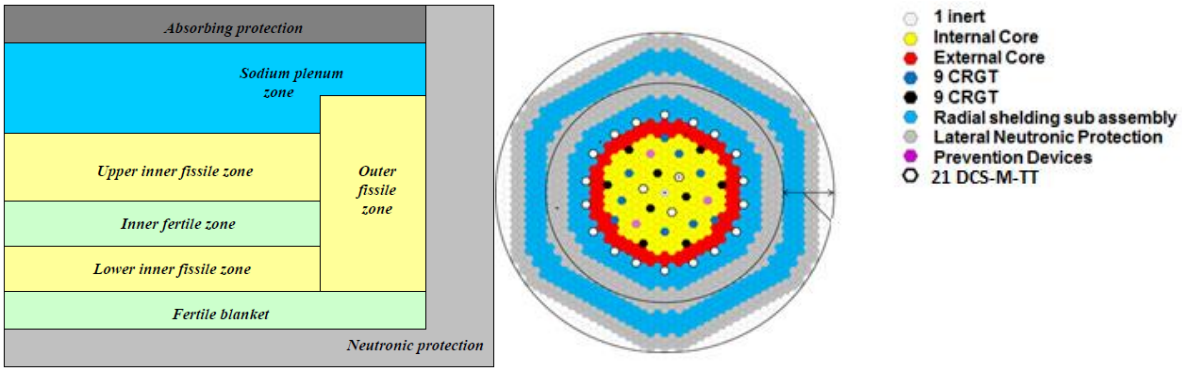

Figure 2: CFV general core geometry. On the left: radial cut - at the center the inner zone is called C1 and C2 is the outer zone at the periphery. In the right: horizontal cut.

In the framework of safety studies dedicated to this new core conceptual design, mitigation studies postulate an initial degraded core state, presented in Figure 3 and Figure 4.

This degraded state has been obtained from two different accidental transients: a mild Unprotected Transient OverPower (UTOP) accident (Bertrand et al. 2016) and an Unprotected Loss of Flow (ULOF) accident calculated with SIMMER-III code (Bachrata et al. 2014 a). This common degraded core state presents two molten zones, one in each of the two fissile zones of the inner core (named C1). However, because of their lower power, the fertile zone of the inner core (between the two fissile zones), as well as the outer fissile zone (named C2), are not molten yet. This inner fertile zone consists of hot degraded debris having collapsed over the bottom fissile zone. Between the fertile and the bottom fissile zones of the inner core, a plug of solidified materials is assumed to be formed based on past experimental evidences (Kayser et al. 1998). The formation of such a plug is also possible above the top fissile zone owing to molten material draining upwards by vapour flow and refreezing in the narrow spaces between the upper neutron protections (PNS) rods still in place. The uppermost zone above the top fissile zone could be filled of materials vapour or liquid sodium depending on the transient and more particularly on the core power level.

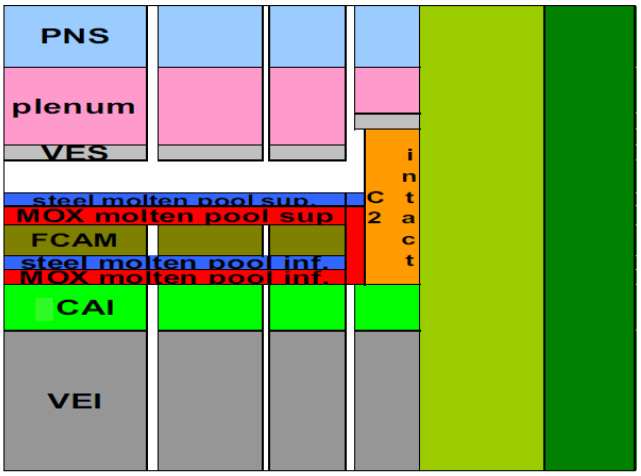

Legend	medium name	temperature	comment
	VEI	900°C	
	void	900°C	
	CAI	900°C	
	molten steel	2700°C	
	molten MOX	2770°C	enrichment PuO2/(U+Pu)O2 = 22,80%
	VES	900°C	
	PLENUM	900°C	
	PNLA	900°C	reflector
	PNLB	900°C	protection
	PNS	900°C	
	FCAM	2400°C	blanket w/o clad (40,85%UO2 + 59,15%void)
	C2	2000°C	

Figure 3: Horizontal cut of the degraded configurations of the CFV core (after a mild UTOP or an ULOF); see the glossary for the abbreviations (Bertrand et al. 2016).

Corresponding author: nathalie.marie@cea.fr

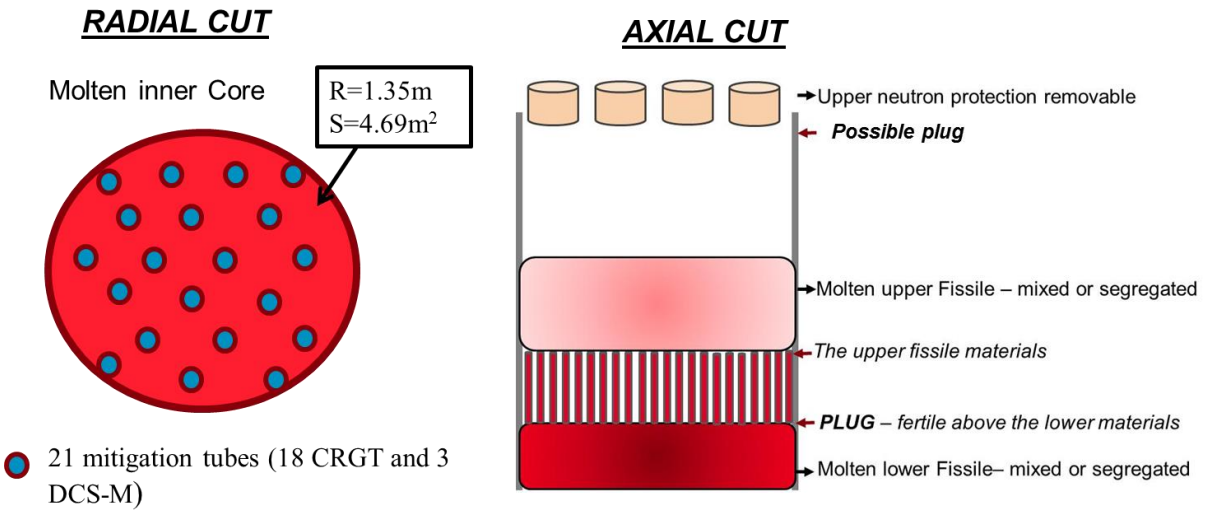

Figure 4: Scheme of the considered initial degraded state (radial and axial cuts) of only the inner core. 21 mitigations tubes are in the inner core (3 DCS-M-TT and 18 CRGT).

The ASTRID CFV core is controlled with 9 control rods and 9 shutdown rods (named CRGT in Figure 2). These 18 CRGT, located inside the inner core, allow corium relocation in their lower part and are useful for severe accident mitigation. Then, 3 additional shutdown rods are devoted to severe accident prevention based on hydraulic passive insertion when the sodium flow decreases. They are named Prevention Devices in Figure 2 (or DCS-P-H) and are not considered in mitigation evaluations. In addition, 21 transfer tubes run across the core diagrid and the strongback down to the core catcher region (called DCS-M-TT in Figure 2 and depicted in Figure 5 - 3 DCS-M-TT are inside the inner core and 18 at the periphery of the core). Of course, any fuel displacement has an impact on the core power evolution. These transfer tubes DCS-M-TT are innovative reactor features exclusively devoted to mitigation purpose. They enable to discharge molten materials from the core directly to the core catcher. In the considered initial degraded configuration where the two fissile zones of the inner cores are molten **(**Figure 3), these 21 transfer tubes and 9 CRGT in the core region have not melted yet (because cooled by inner sodium).

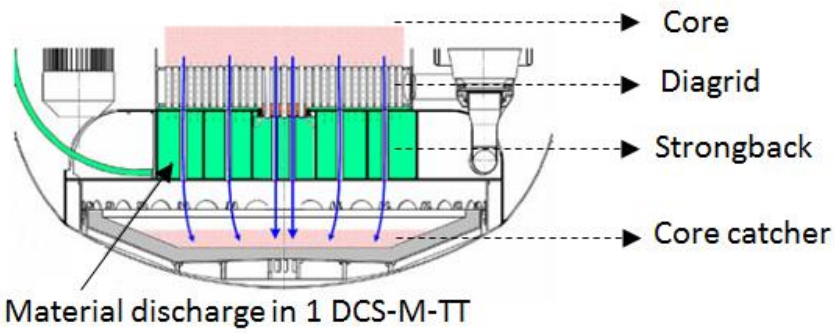

Figure 5: Scheme of mitigation tubes DCS-M-TT crossing the core diagrid and strongback down to the core catcher region

Corresponding author: nathalie.marie@cea.fr

To study the variability of mitigation scenario and the interest of these transfer tubes, a dedicated physical tool is being developed. The physical models are described in the next section.

3 Physical models

The physical models and the calculation scheme of the physical tool handle the coupling between the thermalhydraulics of molten materials located inside each fissile zones and the evolution of the global core neutronics. This tool is parametrized to carry out sensitivity evaluations to epistemic uncertainties (such as the configuration of the degraded core at the beginning of the secondary phase, e.g. molten masses, spatial distribution of materials, fuel power…) or to random uncertainties (such as the not well known physical parameters, e.g. motions of materials inside the pools, the convective heat fluxes…). In a near future, this variable parametrization will enable uncertainty propagation studies.

3.1 Pool models

As depicted in Figure 3 and Figure 4, the two fissile zones in the inner core are molten for the considered degraded state. In each of these zones, the thermalhydraulic evolution of a pool of molten steel and fuel is evaluated using a model which is common to the various molten pools of constant radius. **This model** is applied for the calculation of the molten pool materials evolution inside **both the top and bottom fissile zones**.

Such a molten pool within either the top or bottom fissile zone, composed of steel and fuel, could take different configurations. Indeed the spatial distribution of steel and fuel materials inside the pool evolves during the transient depending in particular on material temperature. Based on literature survey on fuel/steel pool configurations (M. Epstein et al. 1981), various pool configurations are possible (Figure 6).

Each pool of steel and fuel molten materials is described by two layers: a lower mixed steel and fuel layer and a pure upper steel layer. Thus the possible encountered pool configurations are:

- A totally separated configuration, where a steel layer is above a pure fuel lower layer owing to density differences;
- A partially separated configuration where the steel mass is distributed between a pure steel layer which is above and a lower mixed steel/fuel layer;
- An entirely mixed configuration where the pure steel layer does not exist anymore.

If it exists, the lower mixed layer is considered as a homogeneous medium.

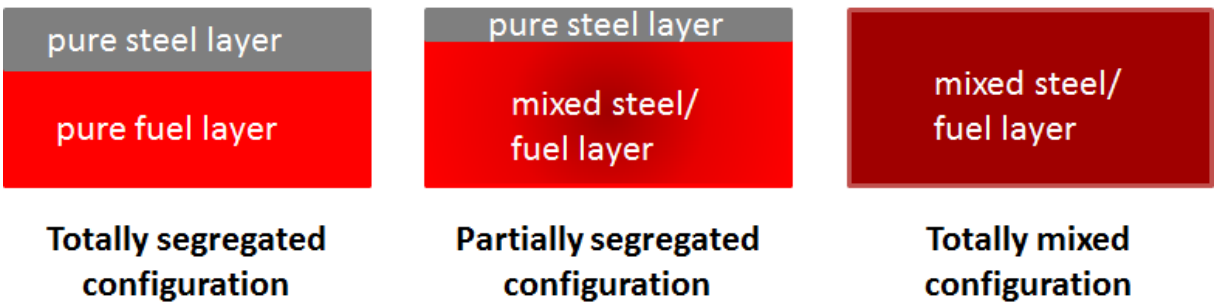

Figure 6: Configurations of molten materials distribution inside a pool (which could be either in the bottom or top fissile zone)

Corresponding author: nathalie.marie@cea.fr

The evolution of the pool configuration is taken into account through models of segregation and mixing of the steel/fuel materials. Based on literature review (Epstein et al. 1981) (Schmizu et al., 1988), a model of mixing caused by boiling of the lower layer, in which the heat is dissipated, has been considered. Owing to the disturbances of layers interfaces caused by boiling, some steel from the upper layer penetrates into the hotter lower layer where it vaporizes enhancing the boiling. A model of material segregation due to buoyancy and material density difference has been implemented and is activated when boiling stops. This boiling temperature of the mixed lower layer which governs the mixing or segregation has been evaluated thanks to thermodynamic calculations using the TAF-ID database developed in the framework of an OECD databank project (Thermodynamics of Advanced Fuels – International Database (TAF-ID) Project Thermodynamics of Advanced Fuels). The composition of the iron based alloy considers three of the major components (Fe-Ni-Cr) of the stainless steel; the compositions of the alloying elements are $Fe_{0.71}Cr_{0.18}Ni_{0.11}$ in mass fractions. The mixed oxide fuel is considered stoichiometric with plutonium content of 20%: $(U_{0.8},Pu_{0.2})O_2$. The overall boiling temperature is close to the steel boiling temperature (≈ 3100K) except when the liquid phase is a nearly pure $(U_{0.8},Pu_{0.2})O_2$ fuel pool; the boiling temperature is then around 3800K as depicted in the boiling line calculated along the $(U_{0.8},Pu_{0.2})O_2$-stainless steel pseudo binary section (Figure 7). Even though this literature review has also led to the definition of ranges of steel mass transfer rates between the two layers (in kg/s), it has also highlighted that steel segregation and mixing depend on various parameters. Indeed, these rates depend on the pool pressure and temperature. It is impossible to fix these rates to a unique value for all the investigated pool configurations. Therefore, they will be treated as parametrized variables. All the more that, these evolutions of materials compositions between the two pool layers highly influence the global core reactivity.

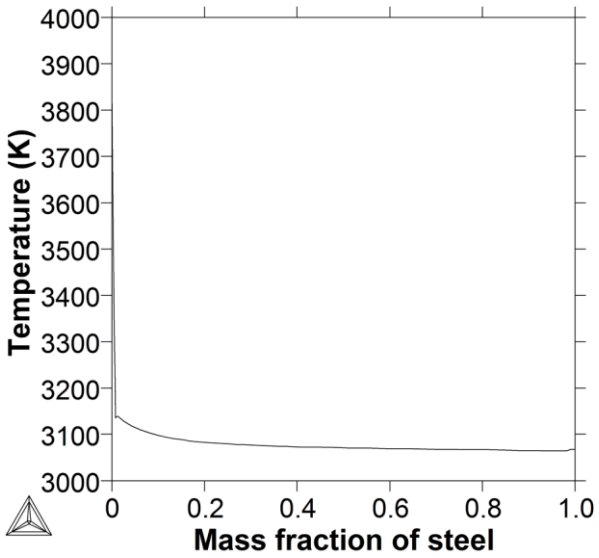

Figure 7: Evolution of the boiling temperature along the pseudo binary section between MOx $(U_{80},Pu_{20})O_2$ and stainless steel $Fe_{0.71}$-$Cr_{0.18}$-$Ni_{0.11}$ (in mass fraction of steel)

Models for the lower layer of each pool located in either the bottom or top fissile zone:

As the fuel and the associated power dissipation is located in the lower layer (the upper layer only contains steel), the evolutions of the materials displacement and temperature in this layer are

Corresponding author: nathalie.marie@cea.fr

simulated as well as the associated global pool axial expansion related to material boiling and steel vaporisation which is at the origin of materials upwards ejection.

The models and equations solved to simulate this lower layer behaviour are given in the following.

Indeed, at each time step, mass, momentum, and energy balances over this volume are solved to evaluate the evolution of the height of the layer (H), the velocity of its upper interface[1] (between lower mixed layer and pure steel layer called V_{max}) and the layer temperature (T), supposed uniform.

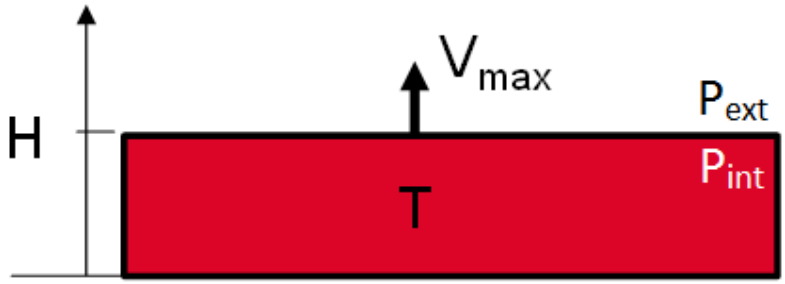

Figure 8: Scheme of the lower layer (pure fuel or mixed steel/fuel) and its main variables (eq. 1)

The resulting set of balance equations governing the lower pool evolution is (Equation 1):

$$\frac{\partial H}{\partial t} = V_{\max} \qquad \text{Equation 1(a)}$$

$$\frac{M}{2}\frac{\partial V_{max}}{\partial t} = -\frac{M}{H}V_{max}^2 - S[P_{ext} - P_{int}] - f\frac{MV_{max}^2}{6D_h} - M_T g \qquad \text{Equation 2(b)}$$

$$MC_p\frac{\Delta T}{\Delta t} = P_{ower} - \sum_i h_i\,(T_{layer} - T_{f,melt})S_i \qquad \text{Equation 3(c)}$$

where M is the total material mass of the lower layer and M_T the mass of the total molten material including also the upper steel layer. P_{ext} and P_{int} are the pressures in the volume above the pool and within the lower layer respectively. P_{int} is the saturation pressure when the lower layer boils. S is the radial pool section and S_i the boundary surfaces around this lower layer (indexed i: lateral along the mitigation tube and horizontal surfaces at the top and bottom of the layer), f is the friction coefficient depending on flow regime (Poiseuille or Blasius correlations). These boundary surfaces are supposed to remain at the fuel melting temperature ($T_{f,melt}$). Indeed, as observed from post-test examinations of SCARABEE (Kayser et al., 1998), the pools are surrounded by their own crust (of refractory oxidic material). The convective heat losses towards the various interfaces of the pool are obtained by Nusselt correlations derived from past experimental tests (Chawla et al. 1982)(Chawla et al. 83). These correlations have been derived in steady-state for one or two phase flows in natural convection. Thus, as our calculations are unsteady, an uncertainty would be associated to these Nusselt numbers in

[1] The velocity of materials is supposed to be unidirectional along the pool height (Z axis) and linear inside the layer: null velocity at Z=0m and maximum velocity at Z=upper interface.

Corresponding author: nathalie.marie@cea.fr

future uncertainty propagation studies. The transient evolution of the fuel crust thickness surrounding the lower pool is also calculated. The released energy due to crust formation is assumed to be supplied to the mitigation tube wall (Φ_{wrap} [W/m^2]) to enhance its melting as expressed by equation 2.

$$\Phi_{wrap} = \underbrace{h_i \left(T_{layer} - T_{f,melt}\right)}_{from\ the\ pool} + \underbrace{L'_{Cf} \frac{de_c}{dt}}_{from\ the\ crust} = \frac{k_f}{e_c}\left(T_{f,melt} - T_{H,neigh}\right) \qquad \text{Equation 2}$$

with k_f the fuel thermal conductivity and e_C the fuel crust thickness [m]. L_{Cf}' [J/kg] is given by $L'_{Cf} = \rho_f\left[L_{Cf} + C_{pf,l}\left(T_{layer} - T_{f,melt}\right) + C_{pf,s}\left(T_{f,melt} - T_{H,neigh}\right)\right]$, L_{Cf} the latent heat of fuel freezing [J/kg], ρ_f the fuel density [kg/m^3], $C_{pf,l}$, $C_{pf,s}$ are the fuel specific heat of liquid and solid phases and $T_{H,neigh}$ the tube wall temperature surface on its exterior side in mitigation tube. The initial crust thickness as well as $T_{H,neigh}$ are input parametrized variables depending on the initial chosen configuration.

Models for the upper layer of each pool located in either the bottom or top fissile zone:

Concerning the upper pure steel layer, only mass and energy balances are solved. The thermal balance equation is solved considering the incoming heat, released from the lower layer through its upper surface, and the heat losses by convection (Chawla et al., 1982) through the lateral and top surfaces. Depending on the user choice, the upper boundary condition could either be a known temperature (crust of steel at melting temperature in case of sodium re-entry and Rayleigh-Bernard convection (Bernaz, 1999) or radiation to the subassemblies structures.

3.2 Other models

This previous model of molten materials pool can handle both unconfined and confined pools. In unconfined pools, the pool cavity is not obstructed at the top. In this case, the pressure above the molten materials remains at the pressure imposed by the reactor design. If the lower layer boils, the pressure inside the lower layer is related to the saturation pressure itself linked to the saturation temperature. This governs the upwards acceleration of the materials. This is the case for pools of materials located inside the top fissile zone if it is not obstructed by relocated materials. Once these pools heat up and some steel is vaporized, the internal pressure of the lower layer increases and its upper interface rapidly rises. The molten materials are then ejected and spread out in the reactor top cavity. At this first step of tool development, it is assumed that these materials do not fall back inside the core, but this will be considered in further developments. On the other hand, a confined pool configuration arises with the re-solidification of molten materials, which could have been drained upwards by sodium vapour, in the upper neutron protection zone where they form plugs located above the VES (upper gas expansion zone) in Figure 3. In this case, the molten materials are confined and the evolution of the saturation pressure versus the temperature is calculated. Thus, there is no large materials vaporization. That prevents molten materials from being ejected upwards.

The failure of the mitigation tubes is modelled either due to thermal or mechanical loading. In case of thermal failure, the heat is convected from the pool to the tube until the total steel thickness is molten. The mechanical rupture is assumed to occur when a threshold value on the difference of pressure between both sides of the tube is exceeded. This threshold value is also parametrized by the user. At this stage of development, as the modelling is zero-dimensional, the failures of the 21 mitigation tubes are simultaneous.

Corresponding author: nathalie.marie@cea.fr

Regarding the mitigation tube wall failure, the initial hole size is a parametrized variable. Once the mitigation tube walls are open, the molten materials are drained away into these tubes. This draining is governed by the over-pressure between the molten pools and the tube and its location depends on the first wall failure elevation given by SCARABEE and BAFOND experimental evidences (Alvarez et al. 1986)(Bede et al. 1993). The discharge rate is thus evaluated according to the pool configuration of molten materials (Figure 9) and the enlarging of the failure opening due to the thermal erosion of the steel tube. Once the volume of the bottom of the CRGT located inside the inner core are full (volume of 1.647 10^{-2} m^3 per tube if we do not take into account the dash-pot or 1.684 10^{-3} m^3 if we do), the materials draining only further continues in the DCS-M-TT tubes.

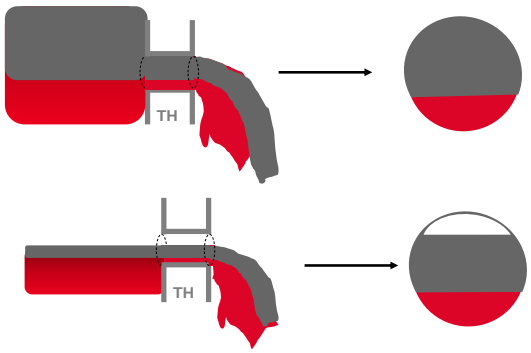

Figure 9 : Illustration of molten materials discharge through the failure opening according to pool configuration (in red the lower layer which could be pure fuel or composed of mixed steel and fuel and in grey the upper pure steel layer)

Finally, as the pools of molten materials configurations in the top and bottom fissile zones (resulting from segregation, mixing, boiling, ejection and draining outside the core) and the Doppler effect influences the global power, the coupling with a neutron kinetics model is required.

A 0D one-group kinetic formulation with 8 groups of delayed neutron precursors is used for the calculation of the delayed neutron population evolution and the associated core global power variation. However, a 0D kinetics model could not handle the influence of the spatial change of geometry (loss of molten materials …) and the spatial deformation of the power distribution. Thus to overcome these lacks, this model is coupled to surrogate models also called metamodels (function of main variables built from numerous simulation results performed with a more complex dedicated code). Indeed, at each time step, the core reactivity, as well as neutronic parameters (power spatial distribution, decay constants of delayed neutrons…) are computed with metamodels, from the various masses distributions in the core, the void fraction and the temperature inside the pools.

These metamodels have been built from ERANOS static neutronic simulations (Ruggeri et al. 2006). For this, 3000 ERANOS simulations have been performed, using a Latin Hypercube Sampling (LHS) design optimized by a space-filling property (McKay, 1979) in order to efficiently investigate the domain of variation of the material distributions. Each ERANOS simulation takes as input the material configuration and computes the corresponding core reactivity, the neutronic parameters for the 0D eight groups model (fractions of delayed neutrons…) and the core power distribution between the fuel inside the top and bottom fissile zones (resulting from the neutron flux axial profile). For each of these outputs, a metamodel has been fitted on the learning sample. Among all the metamodel-based solutions, we focused our attention on the Gaussian process (Gp) metamodel (see Rasmussen & Williams, 2006 for details).

Finally, the Gp metamodel yields a standard deviation of the errors of 10 pcm for the reactivity. A particular time step management has been also implemented to deal with states nearly prompt-critical. The evolution of the decay heat is given by an exponential law established for this core concept.

Corresponding author: nathalie.marie@cea.fr

As no experimental data are still available for complex mixed materials, possibly boiling, pool behaviour and material discharge, pending the SAIGA program, we check in the following part that the results of this 0D physical tool are consistent with 2D SIMMER-III results when considering the same input deck (same test case). The SIMMER-III code (Kondo et al., 2000) is a two-dimensional, multi-velocity field, multi-component, Eulerian fluid-dynamics code coupled with a fuel-pin model and a space-and energy dependent neutron transport kinetics model. A systematic validation of this code is conducting to check the consistency of its results despite the necessary complexity of this code which includes many physical correlations issued from the past researches.

4 Comparison with SIMMER-III results

The initial common degraded core state already described in the section 2 is considered. Values for the various initial parameters, given in this paragraph for the reference case, are the same for the physical tool and SIMMER-III code. These parameters characterize the initial core state resulting from primary accident phase (masses of molten materials in each fissile zone (the fertile is not molten and separates the fissile zones), if the materials are mixed or separated…). To compare the results of the physical tool with SIMMER-III results, we check their consistency regarding variables of interest important for the safety such as reactivity, power and masses discharge. Obviously, all these initial parameters could be changed for sensitivity evaluation purposes.

4.1 Studied cases

Reference case:

For the reference case, the core is assumed at residual power[2] with, at initial time, a zero reactivity (resulting from absorbent fall during the primary accident phase). The degraded configurations in each fissile zone are summarized in Table 1. The upper neutron protections temperature is taken at 1000K. The 21 mitigation tubes (3 DCS-M-TT and 18 CRGT) located inside the inner core have a perimeter of 0.575m each, a cross section of $0.023m^2$ each, a wall thickness of 45mm as well as an initial temperature of 1173K (sodium boiling temperature). The available volume for material relocation inside a CRGT is $1.647.10^{-2}$ m^3. Moreover, the fuel initial crust thickness is 50μm (corresponding to average post-visualisation evidences of SCARABEE tests (G. Kayser et al. 1998)). Considering the top fissile zone, the time needed for the segregation of the total mass of steel, initially mixed with the fuel inside the lower layer, is 13s as highlighted from SIMMER-III results. Conversely, this total mass of steel in the upper steel layer is completely mixed with the fuel lower layer in 7s when boiling occurs. Regarding the bottom fissile zone which is confined, the times need for complete steel mass segregation and the one required for its mixing are 1s, each. This is consistent with SIMMER-III and ranges of values found in literature from analytical evaluations. The mitigation tubes fail consequently to thermal erosion (no mechanical rupture taken into account). The over-pressure due to fission gas if the cavity is confined is taken at 2 bar. When tubes failure occurs, the initial opening of the tube is set to a fairly large value (~30 cm) like in SIMMER-III.

[2] Nominal power is 1500MWth

Corresponding author: nathalie.marie@cea.fr

Parameters	Upper fissile zone	Lower fissile zone
Fuel mass [kg]	7430	5307
Steel Mass [kg]	4910	2052
Confined cavity	NO	YES
Materials	mixed	mixed
Lower layer temperature [K]	3050	3050
Upper layer temperature [K]	No upper layer at the beginning	
Top surface	radiation	Steel crust
Pressure [bar]	1.7	2

Table 1: Parameters of configurations of materials within the top and bottom fissile zones

The SIMMER-III calculation starts with an initial degraded state similar to the one considered, with the same concentration in neutron precursors (Figure 10).

Alternative cases (displayed in Table 2) are computed from this reference case with the SIMMER-III and the physical tool. Case 2 and 3 are sensitivity studies to the molten material configuration (materials are initially stratified instead of mixed) in the bottom fissile zone (case 2) and the top fissile zone (case 3). For these two test cases, in the physical tool as in SIMMER-III, reactivity is shifted to a zero value at the initial time. The case 4 is similar to the reference case with the reactivity shifted to -2000 pcm at the initial time. This corresponds in SIMMER-III studies to the fall of an absorbent from the upper neutronic protection during the primary accident phase.

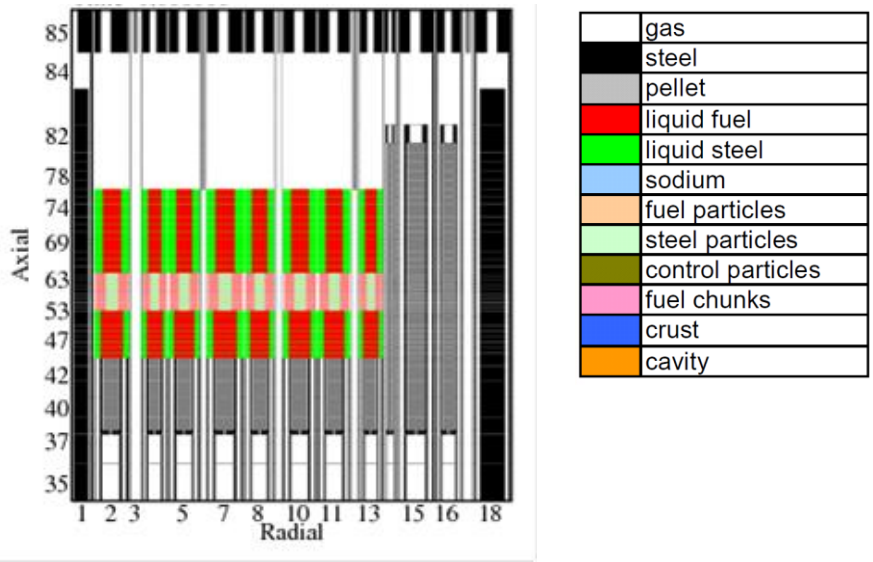

Figure 10: Sketch of the initial state in SIMMER-III nodalization (molten fuel in red, molten steel in green)

Corresponding author: nathalie.marie@cea.fr

Cases	
Case 1	Reference case
Case 2	Reference case but stratified lower fissile zone
Case 3	Reference case but stratified upper fissile zone
Case 4	Reference case with -2000pcm of initial reactivity

Table 2: List of test cases

4.2 Comparison of results

The results obtained with the physical tool are compared to SIMMER-III results on the reference case. The calculated transients are similar regarding the main events occurrences. In the reference case 1, the chronology of different events regarding wrapper failure and material ejection is given in Table 3. Because of the important reactivity insertion caused by steel segregation in the top fissile zone, the core gets prompt-critical (at 0.96s with the physical tool and at 1.17s in SIMMER-III). This is followed by the material upwards ejection from the top fissile zone (immediately in SIMMER-III and 0.25s later with the physical tool). The energy deposition in the pool of molten material in the bottom fissile zone leads to the failure of the mitigation tubes at 1.15s (and an internal pressure around 15 bar) with the tool and at 1.13s with SIMMER-III. In the tool, the discharge of molten materials from the bottom fissile zone governed by this over-pressure is followed by a slight decrease of reactivity. The 18 CRGT tubes are rapidly full at 1.16s. After that, the molten materials only flow inside the 3 DCS-M-TT tubes.

	Physical tool [s]	SIMMER [s]
Prompt criticality (ρ>1$)	0.96	1.17
Wrapper failure (lower fissile zone)	1.15	1.13
Fuel ejection from upper fissile zone	1.21	1.17

Table 3: Transient evolutions in the reference case1

These similar behaviors between results obtained with the physical tool and SIMMER-III are also illustrated in Figure 11 which presents the reactivity evolutions. Globally these reactivity evolutions are consistent.

From static neutronic evaluations (Marie et al. 2015), it has been highlighted, for this degraded configuration of the CFV core, that the complete segregation of steel contained in the **bottom fissile zone**, the other materials distribution being unchanged, induces a drop in reactivity of **-1.40$**. Likewise, the segregation of the steel only in the **top fissile zone** increases the reactivity by **8.09$**.

In the reference case (case 1), the molten steel material mixed in the pools located in the two fissile zones segregates because none of these pools boils. Thus the opposite reactivity effects due to these steel segregation in each zone result first in a global negative variation (in case of SIMMER-III) or very low (with the physical tool) due to the faster segregation of the steel in the bottom fissile zone than in the top fissile zone. Then, when the two material layers are separated inside the bottom fissile zone, only the steel in the top fissile zone goes on to be segregated. This increases the reactivity drastically

Corresponding author: nathalie.marie@cea.fr

and the prompt-criticality is reached. With the prompt-criticality, the power increase is exponential and the materials of the lower layer of pool on each fissile zone (which contains the fuel) quickly heat up (Figure 12). Steel in this layer in the top fissile zone reaches its boiling conditions at 1.05s and is vaporized. Indeed, at that time, in Figure 12 the temperature of the lower layer in the top fissile zone reaches the saturation temperature of steel (3200K). Thus, for the molten materials located in the top fissile zone, on the one hand, the pool lifts up due to steel vaporisation and consequently materials are ejected upwards (at 1.17s with SIMMER-III and 1.21s with the tool). This material dispersion induces a reactivity drop. On the other hand, the boiling stops the steel segregation phenomenon and, in opposite, inducing material mixing which also decreases the global reactivity.

The pool of molten materials in the bottom fissile zone does not boil because it is confined but the pressure increases.

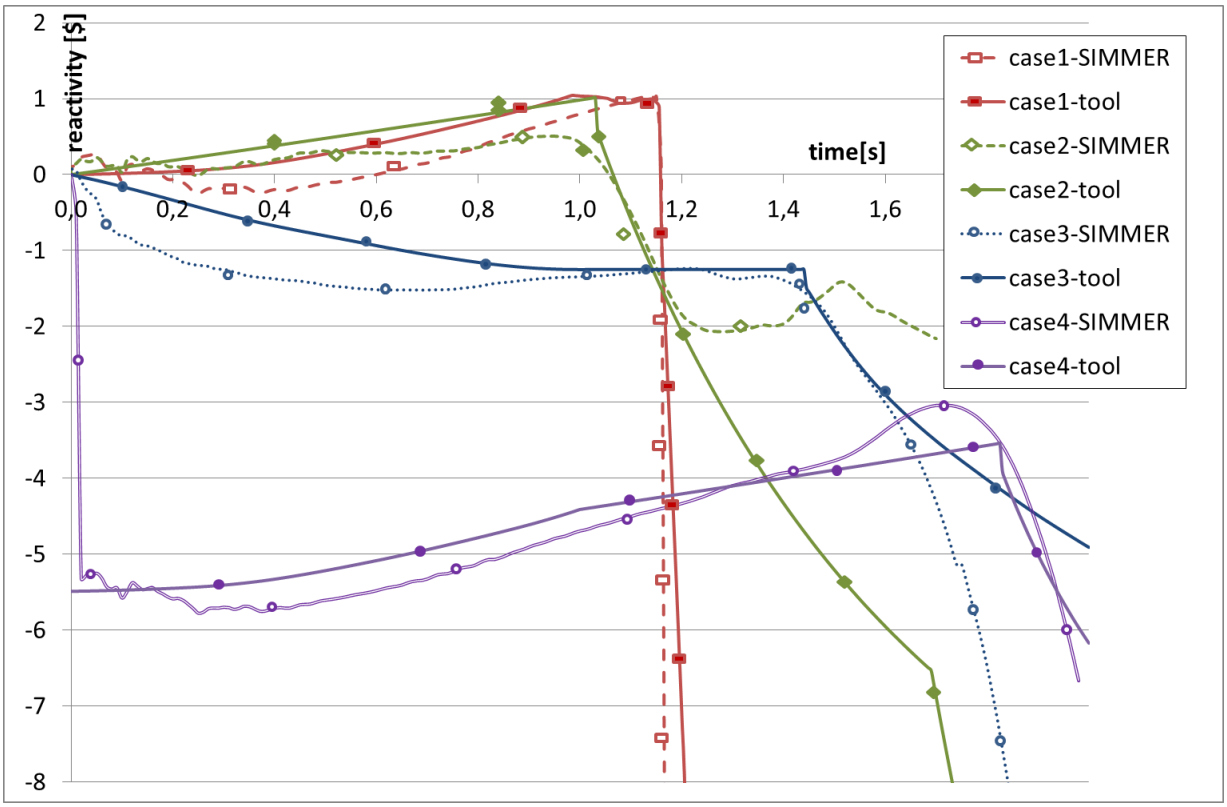

Figure 11: Reactivity evolutions in the various cases

Figure 13 presents the comparison on reference case 1 of power evolutions. The power increase occurs earlier in the physical tool because prompt criticality is reached 0.21 s before with SIMMER-III. At that time, the temperature of the lower layer of each pool rapidly increases (Figure 12). The fuel temperature increasing, the Doppler Effect becomes important and counter-balances the reactivity insertion. At 1.05s the lower layer of the pool located in the top fissile zone boils and the upper steel layer stars to be mixed with the lower layer leading to a slight decrease of the global reactivity and thus of the core power. The materials in the top fissile zone boil, the pool height increases and consequently the reactivity tends to 1$ leading to core prompt-criticality just before materials ejection from the top fissile zone.

Finally, at the end of the reference (case 1) transient calculated with the physical tool, we estimate that, from the initial fuel mass inventory in the fissile zones, 54.3% has been ejected upwards, 37.7% have been discharged downwards and 8% have remained inside the core. In a similar way, from the

Corresponding author: nathalie.marie@cea.fr

initial steel mass inventory in the fissile zones, 66% has been ejected upwards, 11.3% have been discharged downwards and 22.7% are still inside the core.

The agreement between SIMMER-III and the physical tool on this reference case is good but with a discrepancy in the duration between the prompt-criticality and the upwards ejection. Indeed, In SIMMER, the prompt-criticality is instantaneously followed by materials ejection whereas the ejection is delayed by 0.25s with the tool. In SIMMER-III, the whole molten materials are pushed upwards as soon as some steel has locally (in one mesh) reached its saturation temperature. In the tool, this delay corresponds to the time needed to heat-up molten materials to the boiling temperature and to the lift of the layer due to this intensive vaporization up to the upper cavity. At the same time, this fast increase of the fuel temperature induces a high Doppler effect which reduces the power. Furthermore, investigations from BALL-TRAP experiments have shown that around 0.2s of time delay is required for the steel vaporization once its melting temperature[3] is reached (Giot et al. 2010). So finally, the time delay of 0.25s evaluated by the physical tool seems in agreement with this literature result.

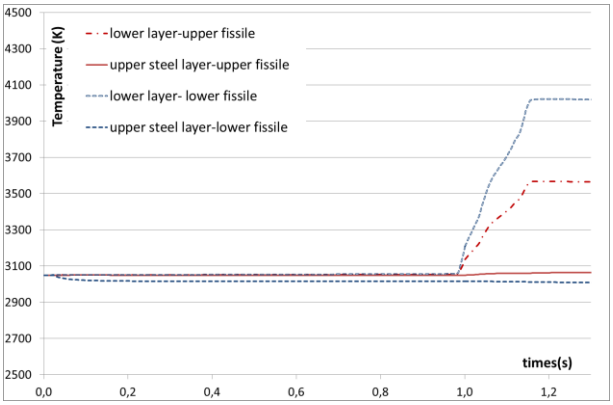

Figure 12: Evolution of the temperature of each layer in the top and bottom fissile zones

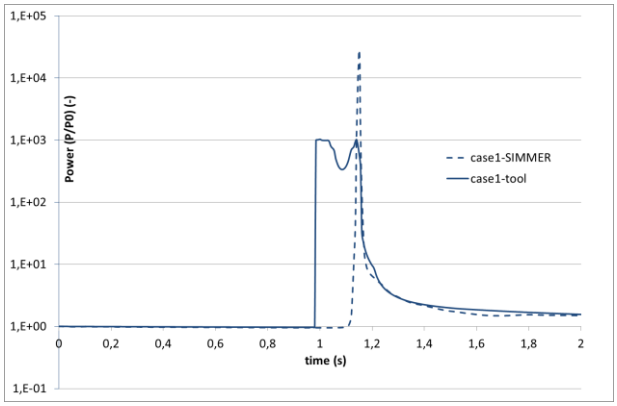

Figure 13: Comparison of power evolutions in the reference case

Regarding the comparison of the reactivity evolutions for the other test cases (Figure 11), the agreement is good between SIMMER-III and the physical tool and this reactivity evolution is consistent with the involved physical phenomena. Thus, in case 2, as the molten materials in the bottom fissile zone are already separated, only materials inside the top fissile zone segregate. The segregation of

[3] Under lower power than that of this case.

Corresponding author: nathalie.marie@cea.fr

steel in this top fissile zone induces a high supply of reactivity. The first seconds in the transient, the reactivity is more important in case 2 than in case 1 for both calculations (the physical tool and SIMMER-III). At 1,03s the walls of the duct fail in the physical tool and materials are discharged downwards inside the mitigation tubes, leading to a global reactivity decrease. The materials discharge is fast until the 18 CRGT are full (at 1.04s) and then the draining in the remaining three DCS-M-TT tubes is slowed down. At 1.2s the draining is stopped in SIMMER-III because of particles blockage inside the ducts.

On the contrary, in case 3, as the molten materials in the top fissile zone are already separated, only materials inside the bottom fissile zone segregate inserting negative reactivity. These behaviours are well observed in both calculation results (SIMMER-III and tool) although the negative reactivity supply is more important at the beginning in SIMMER-III. At around 1.4s, the ducts wall fails in the physical tool and SIMMER-III and the materials flow inside the mitigation tubes.

From the two test cases 2 and 3, it can be concluded that, when both fissile zones are mixed, it is mainly the transient segregation in the top fissile zone which governs the transient.

In case 4, an initial reactivity of -5.49$ is considered due to absorbent insertion during the primary accident phase. Materials in both fissile zones are initially mixed and segregate. The reactivity evolution obtained with the tool is very similar to the one of SIMMER-III. Then, the ducts walls fail at 1.82s enabling materials discharge.

Finally, from the previous results we can conclude that the results of the physical tool are consistent with SIMMER-III results considering the same input parameters. Obviously this comparison work should be expanded to provide confidence in the models before doing sensitivity studies, with the objective of assessing the parameters having the largest impact on the driving physical mechanisms.

In the next section, a first parametric study involving an insertion of negative reactivity and mitigation features illustrates a possible application of this physical tool to the statistical treatments of uncertainties, with the objective of guiding the conceptual design work of mitigation devices.

5 Sensitivity studies Initial insertion of negative reactivity and mitigation features

Thanks to this parametrized physical tool, requiring low CPU time, numerous sensitivity studies could be carried out to investigate various transient behaviours linked to parametrized variables and provide preliminary information for the reactor core design.

By performing sensitivity studies with the physical tool, we can derive an order of magnitude of the average amount of initial negative reactivity which is required to avoid prompt-criticality in the reference case. Thus, from the Figure 14, an initial insertion of -0.4$ seems to be sufficient to avoid prompt-criticality in the reference case 1 whereas -0.3$ is not enough. This type of information can help to quantify the required mass of B_4C falling naturally into the core from degraded Upper Neutronic Protection (PNS) required to avoid prompt-criticality.

Corresponding author: nathalie.marie@cea.fr

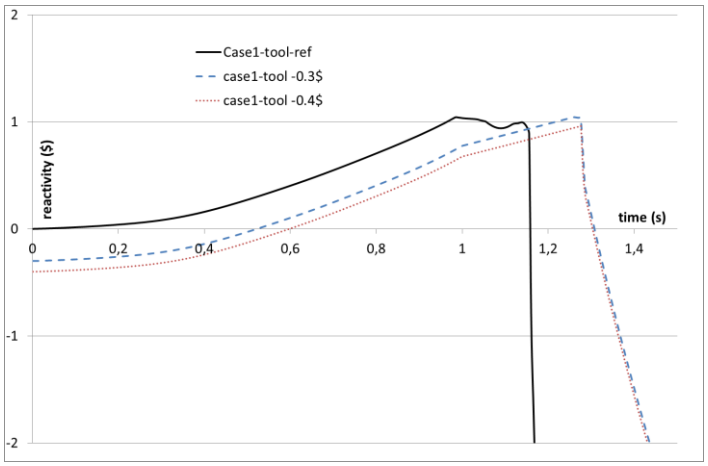

Figure 14: Evolution of reactivity according to absorbent insertion.

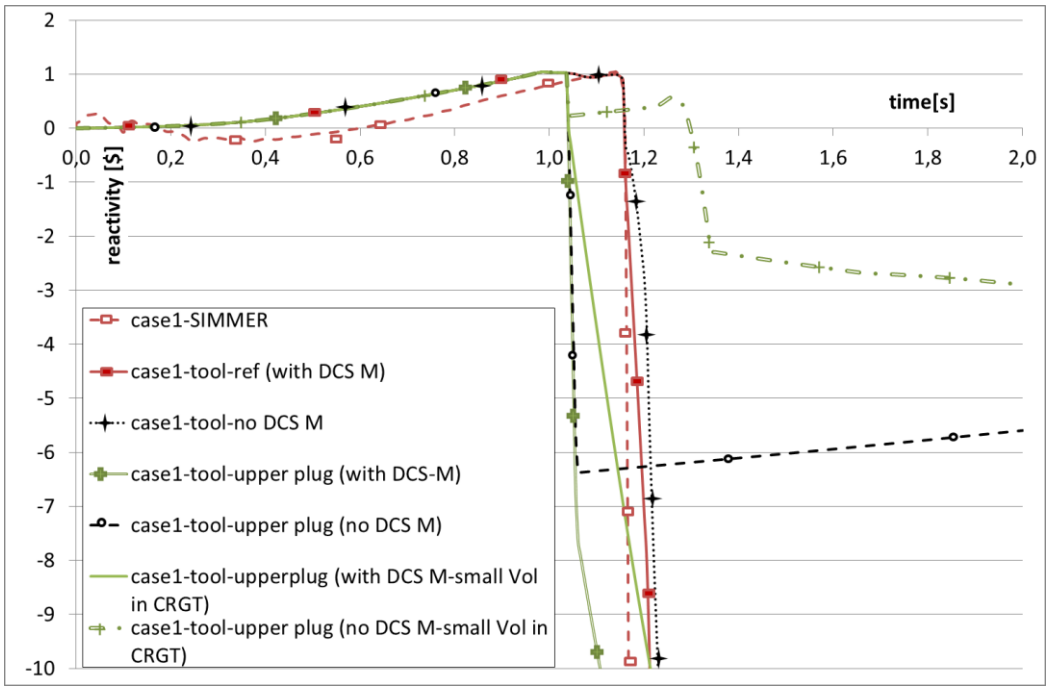

Figure 15: Evolution of reactivity with mitigation features.

This tool enables also to study the influence of mitigation devices on accidental transients. The 21 mitigation tubes considered inside the internal core are composed of 18 control rod guide tubes (CRGT) which could only contain between 1.684 $10^{-3}m^3$ and 1.647 $10^{-2}m^3$ each of molten materials and 3 DCS-M-TT tubes which directly discharge molten materials over the core catcher. The importance of taking into account DCS-M-TT tubes inside the inner core is highlighted by comparing accidental transient evolutions when no DCS-M-TT is placed inside the inner core. Indeed, in the absence of DCS-M-TT in the core, once the CRGT volumes are full, the molten materials remain inside the two fissile zones. The reactivity evolutions are presented in Figure 14 in the reference case 1, and in a case similar to case 1 but with an additional uppermost plug. This situation could arise if molten materials, drained upwards by some vapour flow, are frozen in the colder uppermost locations, leading to a tight plug. In this case, the material could not be ejected upwards and the pressure would increase in this confined zone with the rise of the temperature.

Corresponding author: nathalie.marie@cea.fr

In this reference case 1, the absence of DCS-M-TT inside the inner core would not change much the transient because the dispersion of the materials from the top fissile zone by ejection is enough to drastically decrease the reactivity.

The higher impact of the presence of the DCS-M-TT is observed on the modified case 1 where the top zone is obstructed. In this case with 3 DCS-M-TT tubes, because the top zone becomes pressurized, the tubes failures are sooner and the draining flow rate is larger than in case1 (Figure 14-). If no DCS-M-TT exists inside the inner core and a large volume of 1.647 $10^{-2}m^3$/per CRGT is available for material relocation, this discharge in the CRGT volume is enough to decrease the reactivity to -6$. If the available volume inside the CRGT is only of 1.684 $10^{-3}m^3$ because of the presence of the dash-pot and no DCS-M-TT are considered (last curve in **Figure 15**) the tube failures occur at 1.04s and the materials are discharged until the CGRT are full. This leads to a slight depressurization of the top fissile zone. At 1.05s, the pool in the bottom fissile zone is stratified whereas the pool in the upper fissile zone is still segregated. This leads to a rise of the reactivity which is compensated by the Doppler Effect owing to material temperature increase. At 1.27s the lower layer inside the top fissile zone starts to boil, inducing materials mixing. Large negative reactivity is supplied by this mixing and Doppler Effect. The reactivity becomes negative and the power drops. At 1.35s, the material temperatures remain quite constant and the Doppler Effect vanishes. The global reactivity goes on decreasing due to upper pool mixing up to 2s. Then the pools cool down and the materials of the top fissile zone segregate again after 4s. In this last case without DCS-M-TT, the core remains above its critical state for around 0.25s leading to core powers of 10^3 times the nominal value.

This study shows the benefit of having some DCS-M-TT inside the inner core to rapidly reduce the core power, discharge molten core materials from the core and thus improve safety especially in cases of no upwards materials dispersion.

6 Conclusion and Prospects

In the framework of safety studies devoted to severe accident mitigation in an innovative two fissile zones SFR concept, transfer ducts are introduced into the core region. They run across the core support structure for enhancing molten fuel discharge from disrupted core during the transition and secondary phases of a severe accident. Indeed, as in this core concept potential sodium voiding has a negative neutronic effect, power excursion would be avoided during the primary phase and molten materials would not be massively ejected during this phase. However, a challenge remains: a robust safety demonstration requires showing the efficiency of the mitigation devices to discharge a large amount of fissile materials out of the core region to avoid further energetic recriticality during the transition and secondary phases.

To support the core design, regarding the mitigation features, and assess the advantages of introducing such inner ducts inside the core, an physical tool devoted to the behaviour of molten pools issue is under development. This 0D tool is presented in this paper. It handles heat transfers from molten pools to mitigation tube wall, fuel crust evolution, segregation/mixing of materials (fuel/steel), radial thermal erosion of tube wall or mechanical failure and discharge of molten material with axial thermal erosion of the mitigation tube, coupled with core evolution of the power. This tool is part of a set of tools developed by CEA to carry out uncertainty studies in complement to the use of mechanistic codes requiring high CPU times such as SIMMER-III. Indeed, combining such low dimensional physical tool to

Corresponding author: nathalie.marie@cea.fr

several advanced statistical technics, global sensitivity analyses of the mitigation scenarios become feasible. The main objectives are, on the one hand, to get the variability of the main results of interest for the safety and, on the other hand, to identify the most influential variables for the safety analysis.

As no dedicated experimental results are yet available for complex mixed materials, possibly boiling, pool behaviour and material discharge, this tool has been compared with 2D SIMMER-III calculations including a space-and energy-dependent neutron transport kinetics model. Several test cases results have been compared considering various molten material initial distributions or initial reactivity. The transient evolutions calculated with the tool and SIMMER-III are consistent and the same reactivity evolutions are observed. In the reference case, the steel segregation inside the top fissile zone induces a large reactivity rise. The power increases exponentially and the steel contained in this zone boils leading to upwards ejection of molten materials from the upper part. On the contrary, the steel segregation inside the bottom fissile zone induces small reactivity drops. As this zone is confined, the molten materials are finally discharged through the mitigation tubes after wall failure. This comparison work should be continued to provide confidence in the models before doing more sensitivity studies, an important objective being to assess the most important parameters corresponding to the driving physical mechanisms.

A preliminary study has shown that some transients (reference case 1 with an uppermost obstruction and small volume available in the CRGT for material relocation) without the fuel discharge through the DCS-M-TT ducts could result in a period of high power in the reactor core and an occurrence of possible recriticalities regardless of the fuel discharge through the control-rod guide tube.

This highlights the potentiality of this physical tool for future statistical treatments of uncertainties which could guide the conceptual design of mitigation devices.

Acknowledgment

The authors would like to thank the Generation IV reactor program of the industrial nuclear support and innovation Division of CEA which supports this work as well as the SFR R&D Project.

References

D. Alvarez, P. Malterre, J.M. Seiler, 1986, Natural convection in volume heated liquid pools – the BAFOND experiments: proposal for new correlations, Science and Technology of fast reactor safety, BNES, London.

A. Bachrata, F. Bertrand, D. Lemasson, 2014 a, Unprotected Loss of Flow simulation on ASTRID CFV V3 reactor core, ICAPP 2015, Nice, France, May 3-6, 2015.

A. Bachrata, N. Marie, F. Bertrand, J. B. Droin, Improvement of Model for SIMMER Code for SFR Corium Relocation Studies, 2014 b, International Journal of Mathematical, Computational, Natural and Physical Engineering, International Scholarly and Scientific Research & Innovation 8(3) 521-526.

M. Bede, C. Perret, H. Pretrel, J.M. Seiler, 1993, One component, volume heated, boiling pool Thermohydraulics. 6th Topical International Meeting on Nuclear Reactor Thermal-Hydraulics (NURETH-6), Grenoble, France, October 5-8.

Corresponding author: nathalie.marie@cea.fr

L. Bernaz, 1999, Investigation of natural convection heat transfer to the cooled top boundary of a heated pool, 9th Topical International Meeting on Nuclear Reactor Thermal-Hydraulics (NURETH-9), San Francisco, California, October 3-9.

F. Bertrand, N. Marie, G. Prulhière, J. Lecerf, JM. Seiler, 2016, Comparison of the behaviour of two core designs for ASTRID in case of severe accidents, Nuclear Engineering and Design, Nuclear Engineering and Design, 297, 327–342.

T.C Chawla, S.H. Chan, 1982, Heat transfer from vertical/inclined boundaries of heat generating boiling pools, Journal of heat transfer, 104, 465.

T.C. Chawla, J.D. Bringle, 1983, Downward heat transfer from heat generating boiling pools pertaining to pahr and transition phase, article de conference 831047-68.

M.S. Chenaud , N. Devictor, G. Mignot, F. Varaine, C. Vénard, L. Martin, M. Phelip, D. Lorenzo, F. Serre, F. Bertrand, N. Alpy, M. Le Flem, P. Gavoille, R. Lavastre, P. Richard, D. Verrier, D. Schmitt, Status of the ASTRID core at the end of the pre-conceptual design phase 1, 2013, Nuclear Engineering and technology, 45, 6, 721-730.

Droin J.B., Marie N., Bertrand F., Merle-Lucotte E., physico-probabilistic modelling of the primary phase of an Unprotected Loss Of Flow, NURETH-16**,** Hyatt Regency Chicago, Chicago, IL, USA, August 30-September 4, 2015.

M. Epstein, D.J. Petrie, J.H Linehan, G.A Lambert, D.H. Cho, 1981, incipient stratification and mixing in aerated liquid-liquid mixtures, Chem. Eng. Sci. 36, 4, 84-87.

M. Giot, J. Chipot, G. Labadie, J. Magill, J.-P. Nabot, 2010; SNE-TP – Working Group ETKM – Subgroup 4 Current and Future Uses of Nuclear Infrastructure in Europe February 2010.

G. Kayser, J. Charpenel, C. Jamond, 1998, Synthesis of SCARABEE-N program, with main results and application to the total instantaneous blockage reactor. Nuclear Engineering and Design, 128, 144-185.

Sa Kondo et al., 2000, Phase 2 code assessment of SIMMER-III, JNC TN9400, 105.

W. Maschek and D. Struwe, 2000. Accident Analyses and passive Measures Reducing the Consequences of a Core-Melt in CAPRA/CADRA Reactor Cores, Nucl. Eng. and Design, 202, 311-324.

N. Marie, A. Marrel, JM. Seiler, F. Bertrand, (2016) Physico-statistical approach to assess the core damage variability due to a total instantaneous blockage of SFR fuel sub-assembly, Nuclear Engineering and Design, 297,343–353

N. Marie, A. Bachrata, F. Bertrand, 2015, Comparison of an advanced analytical tool with the SIMMER code to support ASTRID sever accident mitigation studies, NURETH-16, Hyatt Regency Chicago, Chicago, IL, USA, August 30-September 4, 2015.

MD McKay, WJ Conover, RJ Beckman, 1979, A comparison of three methods for selecting values of input variables in the analysis of output from a computer code. Technometrics; 21:239–45.

G. Prulhière, F. Bertrand, B. Maliverney, 2014, Comparison of the reactivity evolutions of heterogeneous and classical ASTRID cores during severe accidents, ICAPP 2014, Charlotte, USA.

CE. Rasmussen, CKI. Williams, 2006. Gaussian Processes for Machine Learning. The MIT Press.

Corresponding author: nathalie.marie@cea.fr

J.M. Ruggieri, J. Tommasi, J.F. Lebrat, C. Suteau, D. Plisson-Rieunier, C. De Saint Jean G. Rimpault, J.C. Sublet, 2006. ERANOS 2.1: International Code System for GEN IV Fast Reactor. ICAPP 2006, Reno, USA.

Y. Schmizu, Y.H. Mori, 1988, Evaporation of single drops in an immiscible liquid at elevated pressures: experimental study in n-pentan and R 113 drops in water, International Journal of Heat and Mass Transfer, 31 1843-1851.

P. Sciora, D. Blanchet, L. Buiron, B. Fontaine, M. Vanier, F. Varaine, C. Venard, S. Massara, A.C. Scholer, D. Verrier., 2011, Low void effect core design applied on 2400 MWth SFR reactor, proceedings of ICAPP 2011, Nice, France.

F. Serre, F. Bertrand, C. Journeau, C. Suteau, D. Verwaerde, D. Schmitt, B. Farges, Status of the French R&D program on the Severe Accident Issue to Develop GENIV SFRs, , ICAPP 2015, Nice, France, May 3-6, 2015.

Thermodynamics of Advanced Fuels – International Database (TAF-ID) Project, https://www.oecd-nea.org/science/taf-id/

H. Yamano, I. Sato, Y. Tobita, 2012, Development of technical basis in the initiating and transition phases of unprotected events for Level-2 PSA methodology in sodium-cooled fast reactor, Nuclear Engineering and Design, 249; 212-227.

H.U. Wider et al., 1982, Status and validation of the SAS4A analysis code system, proceedings of LMFBR Safety Topical Meeting, Lyon.

Corresponding author: nathalie.marie@cea.fr